Draft version March 12, 2018
Typeset using LaTeX twocolumn style in AASTeX61

LOW FREQUENCY VIEW OF GW 170817/GRB 170817A WITH THE GIANT METREWAVE RADIO TELESCOPE

L. Resmi,[1] S. Schulze,[2] C. H. Ishwara-Chandra,[3,4] K. Misra,[5] J. Buchner,[6] M. De Pasquale,[7] R. Sánchez-Ramírez,[8,9] S. Klose,[10] S. Kim,[11,12] N. R. Tanvir,[13] and P. T. O'Brien[13]

[1] *Indian Institute of Space Science & Technology, Trivandrum 695547, India*
[2] *Department of Particle Physics and Astrophysics, Weizmann Institute of Science, Rehovot 761000, Israel*
[3] *National Center for Radio Astrophysics, Pune 411007, India*
[4] *Inter-University Institute of Data Intensive Astronomy, and Dept. of Astronomy, Univ. of Cape Town, Cape Town 7700, South Africa*
[5] *Aryabhatta Research Institute of observational sciencES (ARIES), Manora Peak, Nainital 263 001, India*
[6] *Pontificia Universidad Católica de Chile, Instituto de Astrofísica, Casilla 306, Santiago 22, Chile*
[7] *Department of Astronomy and Space Sciences, Istanbul University, 34119 Beyazıt, Istanbul, Turkey*
[8] *INAF, Istituto di Astrofisica e Planetologia Spaziali, Via Fosso del Cavaliere 100, I-00133 Roma, Italy*
[9] *Instituto de Astrofísica de Andalucía (IAA-CSIC), Glorieta de la Astronomía s/n, E-18008, Granada, Spain.*
[10] *Thüringer Landessternwarte, Sternwarte 5, 07778 Tautenburg, Germany*
[11] *Instituto de Astrofísica and Centro de Astroingeniería, Facultad de Física, Pontificia Universidad Católica de Chile, Casilla 306, Santiago 22, Chile*
[12] *Max-Planck-Institut für Astronomie Königstuhl 17 D-69117 Heidelberg, Germany*
[13] *Department of Physics and Astronomy, University of Leicester, University Road, Leicester, LE1 7RH, United Kingdom*

ABSTRACT

The short gamma-ray burst (GRB) 170817A was the first GRB associated with a gravitational-wave event. Due to the exceptionally low luminosity of the prompt γ-ray and the afterglow emission, the origin of both radiation components is highly debated. The most discussed models for the burst and the afterglow include a regular GRB jet seen off-axis and the emission from the cocoon encompassing a "choked" jet. Here, we report low radio-frequency observations at 610 and 1390 MHz obtained with the Giant Metrewave Radio Telescope (GMRT). Our observations span a range of $\sim$ 7 to $\sim$ 152 days after the burst. The afterglow started to emerge at these low frequencies about 60 days after the burst. The 1390 MHz light curve barely evolved between 60 and 150 days, but its evolution is also marginally consistent with a $F_\nu \propto t^{0.8}$ rise seen in higher frequencies. We model the radio data and archival X-ray, optical and high-frequency radio data with models of top-hat and Gaussian structured GRB jets. We performed a Markov-Chain Monte-Carlo analysis of the structured-jet parameter space. Though highly degenerate, useful bounds on the posterior probability distributions can be obtained. Our bounds of the viewing angle (θ_v) are consistent with that inferred from the gravitational wave signal. We estimate the energy budget in prompt emission to be an order of magnitude lower than that in the afterglow blast-wave.

Corresponding author: L. Resmi
l.resmi@iist.ac.in

1. INTRODUCTION

The LIGO and VIRGO gravitational wave (GW) detectors detected on 17 August 2017 for the first time the emission from two inspiraling neutron stars (GW170817; Abbott et al. 2017b). The 3-dimensional localization inferred from the gravitational wave signal enabled a global network of observers to detect for the very first also electromagnetic radiation emitted during and after the neutron-star in-spiral.

About 1.7 s after the beginning of the neutron-star inspiral, the γ-ray satellite *Fermi* detected a short gamma-ray burst GRB 170817A that also coincided spatially with GW170817 (Goldstein et al. 2017b). As soon as the field became visible from the ground, optical and near IR observations detected a new source in the credible region of GW170817, dubbed AT2017gfo (e.g., Arcavi et al. 2017; Coulter et al. 2017a; Lipunov et al. 2017; Soares-Santos et al. 2017; Tanvir et al. 2017b, for a review see also Abbott et al. 2017a). Radio, sub-mm and X-ray observations revealed no counterpart during the first week after GW170817 (Alexander et al. 2017; Evans et al. 2017; Hallinan et al. 2017; Kim et al. 2017; Margutti et al. 2017b). Only 9 days after GW170817, a new source at the position of AT2017gfo emerged X-ray frequencies (Troja et al. 2017b) and a week later also at radio frequencies (Hallinan et al. 2017).

Modeling the multi-band data revealed two distinct phenomena powering the long-lasting emission from radio to X-ray frequencies. The UV-to-NIR emission up to ~ 30 days originated from radioactive decay of Lanthanides (e.g., Pian et al. 2017; Tanvir et al. 2017b; Evans et al. 2017, for a critical reflection see also Waxman et al. 2017). The emission at longer and shorter wavelengths is of non-thermal origin. The brightness of this component increased since the discovery ($F_\nu \propto t^{0.8}$; Haggard et al. 2017b; Hallinan et al. 2017; Troja et al. 2017b; Mooley et al. 2017a; Margutti et al. 2017b), while the shape of the spectral energy distribution remained constant with time ($F_\nu \propto \nu^{-0.6}$; Mooley et al. 2017a). About 110 days after GW170817, long after the kilonova faded, this source also started to emerge at optical wavelengths (Lyman et al. 2018; Margutti et al. 2018).

Since GW170817 was accompanied by a short-duration GRB, the non-thermal component might naturally be connected with the GRB afterglow but seen off-axis (Granot et al. 2017; Margutti et al. 2017b; Kim et al. 2017; Troja et al. 2017b). However, Kasliwal et al. (2017), Mooley et al. (2017a) and Nakar & Piran (2018) argued that the emission could be produced by the low-luminosity sub-relativistic cocoon. Recently, Hotokezaka et al. (2018) proposed that the observed non-thermal emission could also be produced by the interaction of fast tail of the neutron star ejecta with the circumstellar material.

In this paper, we present our continuing low-frequency observations of the radio transient using the Giant Metrewave Radio Telescope (GMRT), located in Pune, India (§2), covering the time interval from 7 to 152 days after GW170817. The transient started to emerge at 1390 MHz frequencies $\sim$ 67 days after GW170817 and $\sim$ 40 days later also at 610 MHz. We augment our data set with archival X-ray and radio data to model the evolution in the framework of a structured GRB jet. To characterize the highly degenerate multi-dimensional parameter space of the model, we applied the Markov-Chain Monte-Carlo (MCMC) technique. All uncertainties in this paper are quoted at 1σ confidence. We assume the distance to GW170817 to be 42.5 Mpc (Hjorth et al. 2017).

2. OBSERVATIONS AND DATA REDUCTION

2.1. *GMRT observations*

We began monitoring the afterglow of GRB 170817A with the Giant Metrewave Radio telescope (GMRT; Swarup et al. 1991) around a week after the burst (Resmi et al. 2017a). The observations up to 30 days were carried out at L-band with the 32-MHz legacy correlator at 1390 MHz. These early observations yielded only upper limits (Kim et al. 2017) (hereafter Paper-I). We continued our observations through a series of Director's Discretionary Time (DDT) proposals (PI Kuntal Misra), using the upgraded GMRT. On 23 October 2017, 67 days past the burst at 1390 MHz, we secured the first detection at 1390 MHz Each of the observations took about ~ 4 hours duration, including overheads for calibration and slewing. A log of our observations is shown in Table 1.

2.2. *Data analysis*

We processed the wideband data with the COMMON ASTRONOMY SOFTWARE APPLICATIONS (CASA[1]) package (McMullin et al. 2007) and the legacy system data with NRAO ASTRONOMICAL IMAGE PROCESSING SOFTWARE (AIPS[2]) package (Wells 1985). The data were flagged and calibrated using standard procedures. The primary calibrators 3C286 or 3C147 were used as flux and bandpass calibrators and J1248−199 was used for phase calibration. After flux, gain and bandpass calibration, the channel averaging was done to the extent to minimize the effect of bandwidth smearing and target was split. On the target, we performed a few rounds of phase-only self-calibration and afterward a few rounds of amplitude and phase self-calibration.

The beam at 610 MHz has a radius of $\gtrsim 5''$ and is comparable to the distance from the AT2017gfo to the nucleus of its host galaxy.

The flux measurements of the 610 and the 1390 MHz data were obtained from a two-component Gaussian fit (for peak

[1] https://casa.nrao.edu

[2] http://www.aips.nrao.edu

Table 1. Log of GMRT observations of GRB 170817A

Date	$t - t_0$ (days)	F_ν (transient) (μJy)	F_ν (host) (μJy)	beam size (arcsec)
600 MHz				
28-11-2017	102.5	101 ± 20	1134 ± 27	5.61×5.26
22-12-2017	127.0	175 ± 39	991 ± 86	5.98×3.59
1390 MHz				
23-10-2017	66.6	106 ± 19	721 ± 46	4.41×3.05
03-11-2017	77.6	105 ± 17	807 ± 64	2.61×2.19
02-12-2017	106.6	109 ± 14	516 ± 59	3.82×2.45
20-12-2017	124.5	117 ± 19	826 ± 56	2.87×2.16
16-01-2018	151.5	110 ± 14	757 ± 38	2.83×2.15

and underlying baseline) on the final images using JMFIT in AIPS, centered at the afterglow and the galaxy nucleus. Their flux measurements are summarized in Table 1.

2.3. *GMRT Light curve*

Taken in isolation, the GMRT 1390 MHz lightcurve is consistent with a plateau phase (Fig. 1). However, it is also marginally consistent with the $t^{0.8}$ rise previously derived X-ray and high radio frequency observations (Mooley et al. 2018; Margutti et al. 2018). Our last L-band lightcurve extends 152 days after GW 170817, while the latest published high radio frequency observations only extend to 115 days (Margutti et al. 2018). Therefore, the flatness could indeed be a slow turn-over of the afterglow lightcurve, which was not apparent in the high radio frequency observations reported so far. This conclusion is also consistent with the late time X-ray observations reported by Troja & Piro (2018b), where the *Chandra* flux at 158 days is consistent with that at 110 days since burst.

Another possible reason for the plateau phase could also be variabilities as can be seen from Fig. 1. The flux is also found to be variable at X-ray frequencies (Troja & Piro 2018b).

The 610 MHz lightcurve is consistent with both a plateau and a $t^{0.8}$ rise. However, it spans only for a duration of ~ 25 days.

2.4. *Archival data*

We augment our data set with X-ray measurements reported in Margutti et al. (2018), D'Avanzo et al. (2018) and Troja & Piro (2018a), optical observations in reported Lyman et al. (2018), and radio observations reported in Mooley et al. (2018), Margutti et al. (2018) and Troja & Piro (2018a).

3. MODELLING

3.1. *Uniform top-hat jet model*

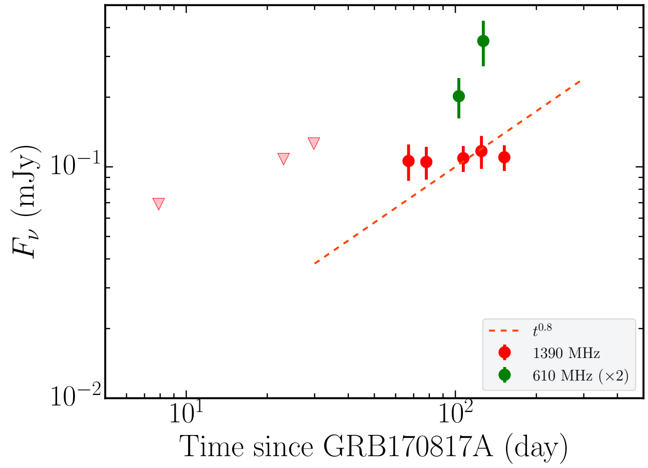

Figure 1. The GMRT observations of the afterglow of GRB 170817A. The observations we report in the paper are given by solid symbols. The 610 MHz points are shifted up by a factor or two. Upper limits are displayed as downward-pointing triangles and were previously reported in Paper-I. The dashed line represents a $t^{0.8}$ rise seen in higher-frequency radio data, over-plotted with 1390 MHz data.

In Paper-I, we used the results from the high-resolution two-dimensional relativistic hydrodynamical code BOXFIT version 2 (van Eerten et al. 2012) to interpret the multi-band afterglow under the ambit of the uniform top-hat jet model. Along with the data, in that paper we presented two out of the several plausible solutions: (i) a narrow jet of half-opening angle $\sim 5°$ misaligned at $\sim 17°$ from the observer, and (ii) a wide jet, of opening angle $\sim 20°$ with the jet axis $41°$ away from the observer line of sight.

However, recent observations indicated that the top-hat jet model is insufficient to explain the behavior of the afterglow (Mooley et al. 2018; Margutti et al. 2018). We found that the lateral expansion of the jet led to a steep decay post the peak in top-hat jet models that could fit the early data of the afterglow. We found that a $F_\nu \propto t^{0.8}$ rise lasting for about a decade in time is possible with a uniform top-hat jet. However, the parameters that lead to a $F_\nu \propto t^{0.8}$ phase between $10-100$ days require unreasonably high values of energy and density of the ambient medium, which also lead to fluxes several orders of magnitude larger than observed. A low fraction of accelerated electrons could reduce the flux but that results in high values of γ_m leading to the disagreement with the observed spectrum of the afterglow.

3.2. *Structured-jet model*

In order to explain the evolution of the afterglow, several groups have invoked either a radial (Mooley et al. 2018) or a lateral (Lazzati et al. 2017; Margutti et al. 2018; Lyman et al. 2018) structure in the energy and velocity profile of the outflow. In the radially structured cocoon model, the relativistic jet is "choked" and the burst and the afterglow is believed to originate from a sub-relativistic cocoon (Mooley et al. 2018; Nakar & Piran 2018).

Since evidence for relativistic jets are seen in gamma ray bursts (Frail et al. 1997; Taylor et al. 2004), we investigate the parameter space of a structured relativistic jet to explain the afterglow observations. The Gaussian structured jet we consider is similar to previously discussed by Lazzati et al. (2017), Margutti et al. (2017a), D'Avanzo et al. (2018), Lyman et al. (2018), and (Troja et al. 2018) where the kinetic energy per solid angle ($\mathcal{E}$) has a polar structure given by,

$$\mathcal{E}(\theta) = E_c \exp\left(-\frac{\theta^2}{\theta_c^2}\right), \tag{1}$$

where θ_c is *structure parameter* deciding the sharpness of the angular profile. A large θ_c jet is similar to a uniform jet. To have the same deceleration radius (r_0) across the polar direction, we let the initial bulk Lorentz factor to follow,

$$\Gamma_0\beta_0 = \Gamma_c\beta_c \exp\left(-\frac{\theta^2}{2\theta_c^2}\right), \tag{2}$$

where β is bulk velocity of the jet normalized by the speed of light and Γ the bulk Lorentz-factor of the GRB jet. A jet where the kinetic energy is proportional to $\exp\left(-\theta^2\right)$ and the Lorentz factor is proportional to $\exp\left(-\theta^2/2\right)$ is possible if the ejected mass also follows an angular profile of $\exp\left(-\theta^2/2\right)$, which is a reasonable assumption to make.

Due to the angular structure, the initial jet Lorentz factor decrease towards high latitudes and becomes sub-relativistic towards high latitudes. We assume that the initial jet Lorentz factor follows

$$\Gamma(\theta)\beta(\theta) = \Gamma_0(\theta)\beta_0(\theta)\left(\frac{r}{r_0}\right)^{-3/2} \tag{3}$$

where $r \gg r_0$ can be considered equal to the distance from the center of the explosion. This velocity profile reduces to the Blandford-McKee self-similar solution in the ultra-relativistic limit (Blandford & McKee 1976) and the Sedov-von Neumann-Taylor solution in the non-relativistic limit (Taylor 1950). To simplify the calculation, we assume a rigid jet that does not expand laterally.

To calculate the flux observed by an observer at an angle θ_v from the jet axis, we follow the same formalism developed by Lamb & Kobayashi (2017). We divide the jet into N polar rings of width $\delta\theta = \theta_j/N$, which are further divided into M azimuthal elements, each with a width of $\delta\phi = 2\pi/M$. Direction to the observer's line of sight is taken as the zero of the ϕ coordinate. An element i,k with its central axis at (θ_i, ϕ_k) from the jet axis, is at an inclination $\alpha_{i,k} = \cos\theta_i\cos\theta_v + \sin\theta_i\sin\theta_v\cos\phi_k$ from the observer. As done in Lamb & Kobayashi (2017), we sum the contribution of each of these elements to obtain the total flux observed by the off-axis observer at $t_{\rm obs}$ at a frequency $\nu_{\rm obs}$. For this we interpolate the equation $t_{\rm obs} = \frac{r}{\beta(r)c}\left[1-\beta(r)\cos\alpha_{i,k}\right]$ and find the distance r corresponding to the $t_{\rm obs}$ for each jet element i,k. The off-axis flux from each element is estimated as $a^3 f^{\rm on}{}_{\nu/a,i,k}(r)$, where $a = \frac{1-\beta(r)}{1-\beta(r)\cos\alpha_{i,k}}$ and $f^{\rm on}$ is the flux observed by an observer located on the central axis of the element. Again, we follow Lamb & Kobayashi (2017) to obtain $f^{\rm on}{}_{\nu,i,k}$ as $\frac{L_{\nu,i,k}}{4\pi d_L^2}\frac{\Omega_{i,k}}{\Omega_{e,i,k}}$. Here $\Omega_{e,i,k} = \max\left[\Omega_{i,k}, 2\pi(1-\cos\frac{1}{\Gamma_{i,k}})\right]$ and $\Omega_{i,k} = \int_{\phi_{k-1}}^{\phi_k} d\phi \int_{\theta_{i-1}}^{\theta_i} d\theta \sin\theta$ is the solid angle subtended by an element at a point on its central axis.

The isotropic synchrotron flux $L_\nu/4\pi d_L^2$ is estimated following Sari et al. (1998), with modifications for expressions of the downstream magnetic field, B, and minimum Lorentz factor, γ_m, of the shocked electron population, suitable for the sub-relativistic flow: $B = \sqrt{32\pi m_p c^2 \epsilon_B n_0 \Gamma(\Gamma-1)}$, and $\gamma_m = 1 + \frac{m_p}{m_e}\frac{p-2}{p-1}\epsilon_e(\Gamma-1)$. Here, m_p and m_e are the proton and electron masses, respectively, c is the speed of light, p is the power-law index of the non-thermal electron population, and ϵ_e and ϵ_B are the fractional energy content in the non-thermal electron population and magnetic field, respectively. This formalism assumes a geometrically and optically thin jet. A thin shell assumption is valid, because even the 610-MHz data do not show the signs of self-absorption until now.

Our model has minor differences from other structured-jet models presented in the literature. The angular profile of $\mathcal{E}$ and $\Gamma\beta$ of D'Avanzo et al. (2018) is different from ours, but they use the same dynamical evolution for $\Gamma\beta$. Both D'Avanzo et al. (2018) and Margutti et al. (2018) use a free index (s_1 and α, respectively) to modify the angular structure. Since the afterglow parameter space is heavily degenerate with at least 7 free parameters, we chose to fix the Gaussian profile. The angular profile we use is very similar to Lamb & Kobayashi (2017) except that we let $\mathcal{E} \propto \exp\left(-\frac{\theta^2}{\theta_c^2}\right)$ in order to have a r_0 independent of the jet latitude. Our calculation of the jet dynamics and the equal arrival times differ from Lamb & Kobayashi (2017) who used a $t^{-3/8}$ profile for Γ and scales the observed time by the Doppler factor (a) to obtain the equal arrival times. Since β can be considerably lower than unity, we chose to do the interpolation to obtain the equal arrival time surfaces.

3.3. *Model parameters and the shape of the lightcurve*

The structured jet can be specified with four parameters, E_c, Γ_c, θ_c, and θ_j. The first three parameters were mentioned in the previous section. The last parameter θ_j corresponds to the half-opening angle if there is a hard edge of the jet beyond which the energy sharply drops down.

Similar to top-hat models, Γ_c influences the deceleration time of the jet, and E_c influences both the deceleration time

Table 2. Prior and posterior distributions of the structured-jet afterglow model

Parameter	Prior range	Posterior
$\log(E_c/\mathrm{erg})$	47 – 54	$51.76^{+0.52}_{-0.39}$
Γ_c	30 – 300	$215.4^{+60.3}_{-85.9}$
θ_c (rad)	0.07 – 0.2	$0.12^{+0.04}_{-0.03}$
θ_v (rad)	0.1 – 0.9	$0.47^{+0.15}_{-0.08}$
$\log(n_0/cm^{-3})$	-5 – 2	$-2.68^{+0.88}_{-1.00}$
$\log\epsilon_B$	-5 – -0.5	$-4.37^{+1.10}_{-0.48}$
$\log\epsilon_e$	-2 – -0.5	$-0.66^{+0.13}_{-0.45}$

NOTE—We chose a uniform distribution for each prior. The values of the marginalized posterior distributions represent the median the corresponding 16 and 84 percentiles.

as well as the overall level of flux. Hence we concentrate here on the jet profile θ_c and the jet half-opening angle θ_j. In addition, the observer's viewing angle θ_v also modifies the lightcurve. Figure 2 shows a diverse assembly of lightcurves for different values of θ_j, θ_c, and θ_v.

The half-opening angle θ_j is the least sensitive of all. The jet structure parameter θ_c plays a crucial role in the rise time and the slope of the lightcurve. In addition, along with θ_v, θ_c also influences the peak time. A small θ_c corresponds to a sharply varying profile, where the jet core is far more energetic than its edges, whereas a large θ_c broadly resembles a uniform jet.

3.4. *Parameter estimation*

The parameter space of our afterglow model is 9-dimensional, $\Theta = E_c, \Gamma_c, \theta_c, \theta_j, \theta_v, n_0, \epsilon_B, \epsilon_e, p$. To reduce the number of free parameters, we make two additional assumptions. Firstly, the spectral energy distribution from X-ray to radio frequencies is well described by a simple power law. Following Margutti et al. (2018), we fix the value to $p = 2.17$. Secondly, it is natural to let the profile go towards a polar angle of $\pi/2$. Moreover, we found that the lightcurves are not very sensitive to the value of θ_j (left panel of Fig. 2). No bounds on θ_j could be obtained from our initial MCMC analysis either. Therefore we fixed $\theta_j = 1.2$ rad in our final analysis. We chose a value less than $\pi/2$ to avoid numerical errors in the synchrotron flux calculation that result from extremely low values of jet velocity β. We thus reduced the dimension to 7.

We used the publicly available affine invariant Markov-Chain Monte-Carlo parameter estimation code EMCEE version 2.2.1 (Foreman-Mackey et al. 2013) to obtain the bounds of the parameters consistent with the data. We chose a uniform distribution for the prior of each parameter with the ranges displayed in Table 2 and we generated 1.5×10^6 realizations of the model (500 walkers and 3000 steps). Our results are presented in Fig. 3. To check for convergence, we repeated the simulation multiple times with different initial values of the walkers.

Even though the parameter space is degenerate and the data is not highly constraining (Margutti et al. 2018), we could obtain tight bounds on E_c, n_0, θ_c and θ_v. 16 and 84% quantiles of the posterior correspond to $2 \times 10^{51} < E_c < 2 \times 10^{52}$. Total energy $E_{\rm tot}$ in the jet is given by $\int_0^{2\pi} d\phi \int_0^{\theta_j} d\theta \mathcal{E} \sin\theta$, which leads to

$$E_{\rm tot} = \pi E_c \theta_c^2 \left\{ 1 - \exp\left(-\frac{\theta_j^2}{\theta_c^2} \right) \right\}. \tag{4}$$

Corresponding to the mean of the distribution of θ_c and E_c, $E_{\rm tot} = 2.6 \times 10^{50}$ ergs. The ambient number density, $n_0 \sim 10^{-2}$–10^{-4} cm^{-3}, is consistent with what is expected for short GRB environments (Fong et al. 2015). Our bounds on θ_v are consistent with that from the GW analysis from LIGO/Virgo (Abbott et al. 2017b). We find that a low fraction thermal energy density is deposited in the magnetic field, but the fraction going to electrons are towards the maximum possible limit. We notice a tight constraint between θ_c and θ_v. This comes from the rising slope of the afterglow being tightly constrained by high radio frequencies, as expected from the behavior of the lightcurves seen in Fig. 2. The bulk Lorentz factor is sensitive only to the rise time of afterglow, and hence is not constrained well.

Our bounds on θ_v (27^{+5}_{-5} degree) are within the broad bounds of the LIGO analysis (Abbott et al. 2017). The combined LIGO and DES-SHoES bounds presented in Abbott et al. (2017) is consistent with our posterior. However, the LIGO DES-SH0ES bounds along with our posterior will tightly constrain the value of θ_v between 20° and 33°. The best fit values of θ_v and ϵ_e of Lazzati et al. (2017) is within our posterior bounds, but their n_0 is relatively low, where our bounds are at a higher range; and their ϵ_B is relatively higher than ours. Our posterior is very similar to that of (Troja et al. 2018). We have slightly tighter bounds on $\mathcal{E}, \theta_c, \theta_v$, and n_0. Troja et al. (2018) also vary θ_j and p which we keep fixed. Our bounds on ϵ_B are broader than theirs and also goes down to lower values. The structured-jet parameters D'Avanzo et al. (2018) and Lyman et al. (2018) have used for the lightcurves they present are well within our posterior bounds.

In Fig. 4, we present 100 highest likelihood lightcurves from our model realizations (with similar reduced χ^2 values). The higher radio frequencies dominate the data, and hence the flatness in GMRT 1390 MHz is not reproduced well by the models. θ_v in these 100 realizations are broadly divided into two distribution, one around $\sim 21.5°$ and the other around $\sim 25°$, leading to two classes of lightcurves. The lower θ_v ones decline earlier, by around 500 days while

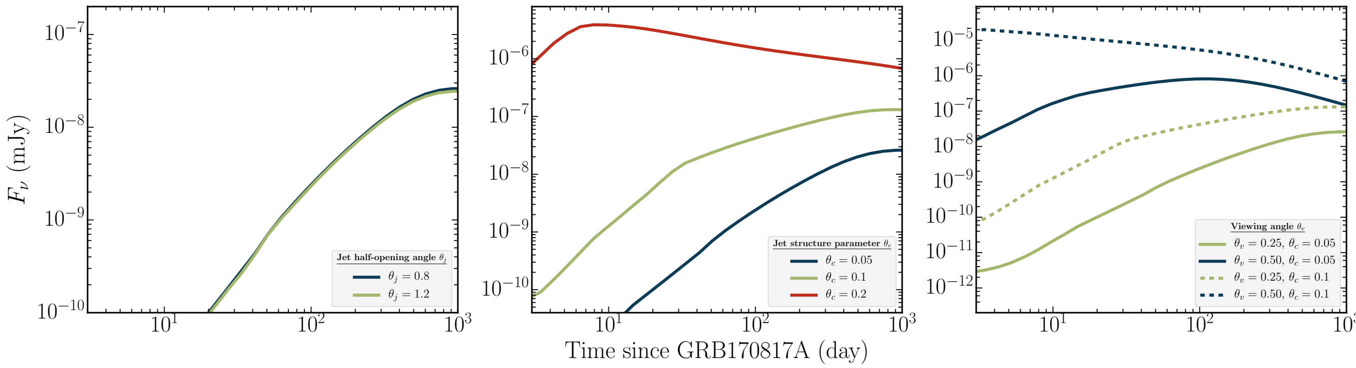

Figure 2. The Sensitivity of lightcurves (3 keV) on the structured-jet parameters. **Left**: Variation in the jet half-opening angle θ_j. An increase in the jet half-opening angle hardly changes the total flux. At large jet angles, the energy content in the Gaussian jet is negligible compared to the central part. For both lightcurves we assumed $\theta_c = 0.05$ rad and $\theta_v = 0.5$ rad. **Middle**: Variation of jet structure parameter θ_c. The slope of the lightcurve before the peak is sensitive to θ_c. The peak time is determined by θ_v and is the same for the blue and the green models. As θ_c gets larger, the lightcurve approaches to that of a uniform jet, and the peak shifts to earlier times. Since all curves have the same energy per solid angle ($\mathcal{E} = 5 \times 10^{51}$), an increase in θ_c leads to higher $E_{\rm tot}$, which is the reason for the higher flux. For these lightcurves, we assumed $\theta_j = 0.8$ rad and $\theta_v = 0.5$ rad. **Right**: Effect of viewing angle for two different θ_c values. A larger viewing angle leads to a later peak. As seen in the middle panel, the pre-peak slope is sensitive to θ_c. The rising phase of the blue dashed curve is steep, but it is out of the x-axis range.

the higher θ_v realization start to decline later. However, late observations at higher frequencies may agree with the flatness in GMRT L-band lightcurve and refine these predictions.

4. CONSTRAINTS FROM PROMPT EMISSION

In the off-axis structured-jet scenario, the properties of the observed prompt emission, particularly the isotropic equivalent energy ($E^{\gamma}_{\rm iso}$), is sensitive to the jet bulk Lorentz factor (Γ_c), jet structure parameter (θ_c), and viewing angle (θ_v) (Donaghy 2006; Yamazaki et al. 2003). Assuming that the burst and the afterglow are produced by an off-axis relativistic jet, further constraints on Γ_c, θ_c, and θ_v can be arrived at in conjunction with the afterglow parameter space. We have carried out the same analysis in paper-I for uniform top-hat jet. Here we extend it to the Gaussian structured jet.

The observed GRB flux, from which the $E^{\gamma}_{\rm iso}$ is derived, is the intensity integrated over the surface of the jet visible to the observer. The flux depends on the viewing angle θ_v of the observer, the energy content of the jet, and the bulk Lorentz factor. In order to obtain $E^{\gamma}_{\rm iso}$, we follow the framework developed by Salafia et al. (2015), who derive, for the isotropic equivalent energy in prompt emission observed by an off-axis observer,

$$E^{\gamma}_{\rm iso}(\theta_v) = \int d\Omega \frac{\delta^3(\alpha)}{\Gamma(\theta)} u^{\gamma}(\theta), \tag{5}$$

where, $\delta(\alpha)$ is the Doppler factor given by $1/\Gamma(1-\beta\cos\alpha)$ and $u^{\gamma}(\theta)$ is the energy per solid angle in prompt emission. The angle α entering in the expression of δ is the same as defined in §3.2; the angle between the observer line of sight and the normal to jet surface at θ, ϕ.

We consider, $u^{\gamma}(\theta)$ to follow the same functional dependence as $\mathcal{E}$, energy per solid angle in the afterglow blast wave (Eq. 1).

$$u^{\gamma}(\theta) = u_c \exp -\frac{\theta^2}{\theta_c^2}. \tag{6}$$

In order to obtain the normalization u_c, which gives the energy per solid angle at the jet axis ($\theta = 0$), we assume that the kinetic energy budget in the afterglow, $E_{\rm tot}$, given in Eq. 4, and the total energy radiated away in prompt emission as measured by an on-axis observer are related by a factor ζ. This assumption is motivated by a constant γ-ray efficiency (Cenko et al. 2011) seen in long GRBs detected by γ-ray triggers, where the observer is very likely to be aligned close to the axis of the jet.

Total isotropic equivalent energy in prompt emission as measured by an on-axis observer is $E^{\gamma}_{\rm iso}(\theta_v = 0)$. Therefore, to obtain u_c,

$$u_c \int_0^{\theta_j} d\Omega \exp\left(-\frac{\theta^2}{\theta_c^2}\right) \frac{\delta^3(\theta_v = 0)}{\Gamma(\theta)} = \zeta \frac{E_{\rm tot}}{(1-\cos\theta_j)}. \tag{7}$$

The factor $(1-\cos\theta_j)$ converts the afterglow energy $E_{\rm tot}$ to isotropic equivalent energy.

We consider the first 5000 of our high likelihood realizations and see whether a given realization can reproduce the observed $E^{\gamma}_{\rm iso}$ (Goldstein et al. 2017b) with reasonable values of ζ. From Cenko et al. (2011), a variation in ζ from 0.05 to 40 is commonly seen, with a mean value being ~ 4.

For the given realization, we first obtain u_c using Eq. 7 after replacing θ_v by 0 and then proceed to obtain $E^{\gamma}_{\rm iso}(\theta_v)$ using Eq. 5. In Figure 5, we display our results for $\zeta = 1$ and $\zeta = 0.1$. We find that the observed Fermi $E^{\gamma}_{\rm iso}$ reported by Goldstein et al. (2017b) can be reproduced if the energy bud-

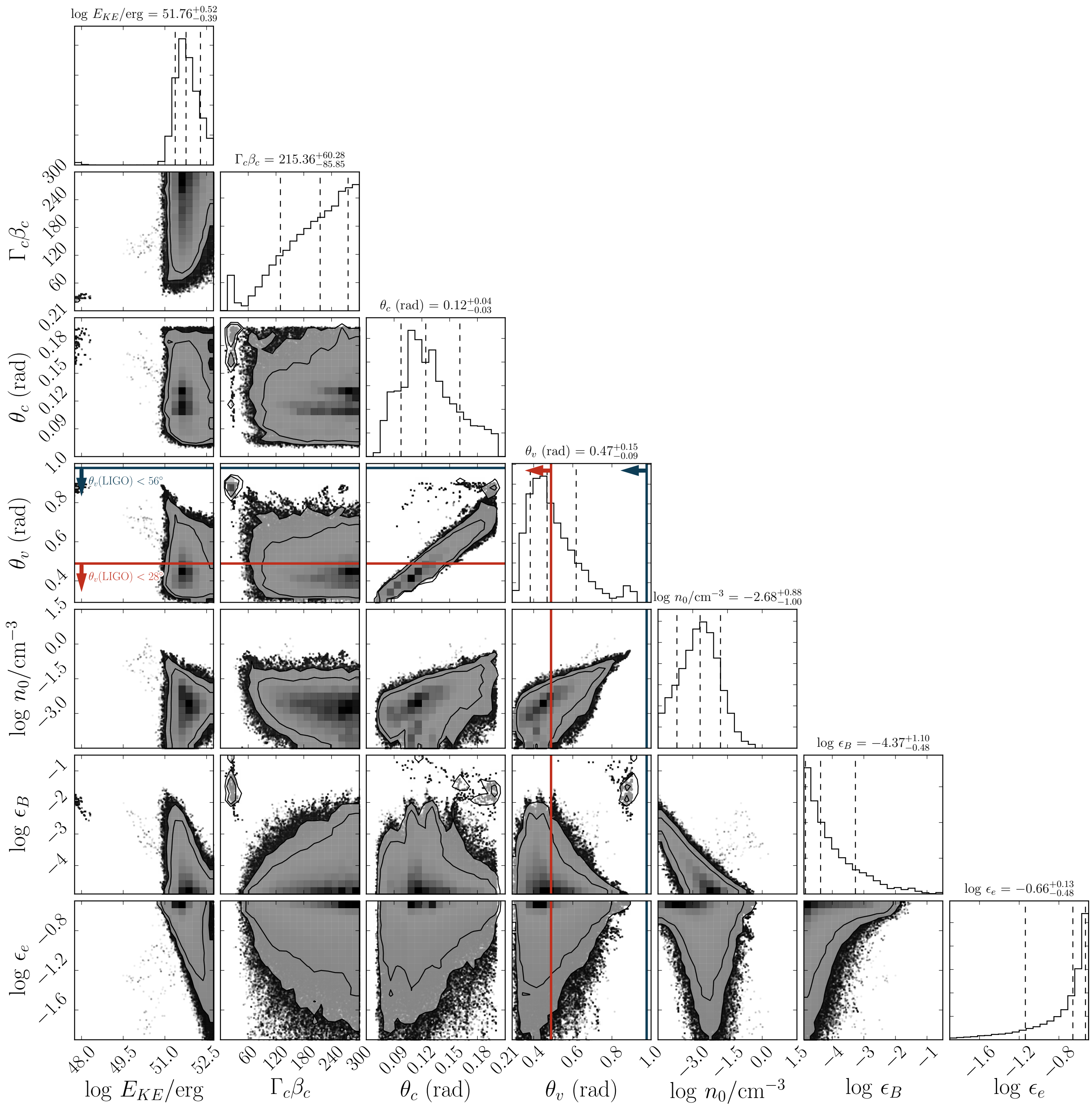

Figure 3. Posterior distributions and degeneracies of the model parameters, after removing the burn-in phase. The median values and their 1σ uncertainties are displayed on top of the marginalized distributions. The blue and red lines display the constraints from the GW signal (Abbott et al. 2017b). The tighter constraint of $\theta_v < 28^\circ$ was derived using a distance of 42.5 Mpc towards NGC4993, the host of GRB 170817A.

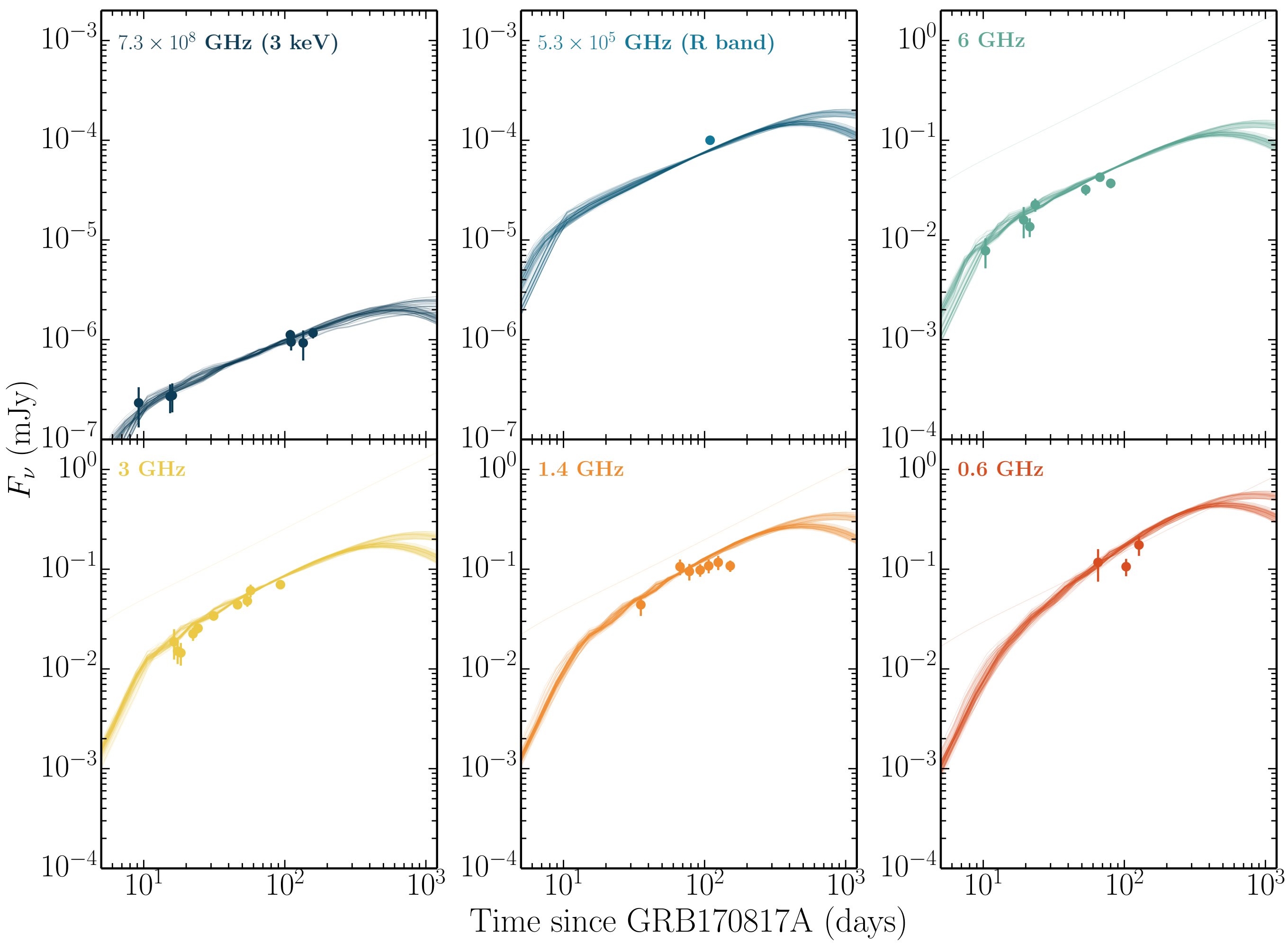

Figure 4. The 610 and 1390 MHz GMRT lightcurves along with higher frequency data from the literature (detections: •, upper limits: ▼). Overlaid are 100 models with similar χ^2 values. Some lightcurves show small-scale undulations, due to the limited resolution in polar directions. The lightcurves that decay earlier, by $\sim$ 500 days have a smaller θ_v than the ones that decay later. Since the data is dominated by higher radio frequencies, the flatness of the GMRT 1390 MHz lightcurve is not well reproduced in the model realizations.

get in prompt emission is of an order of magnitude lower than that in the afterglow. For $\zeta = 1$, i.e., similar energies in the afterglow and prompt emission (i.e., for 50 % γ-ray efficiency), only a few low bulk Lorentz factor solutions can reproduce the observed $E^{\gamma}_{\rm iso}$. However, the ζ required to explain the observations is not unusual of ordinary GRBs (Cenko et al. 2011), and is also supportive of a low efficiency process like internal shocks. This analysis also confirms that a relativistic structured outflow can well describe both prompt and afterglow observations of GRB 170817A.

5. SUMMARY

We present the low radio frequency observations of the afterglow of GRB 170817A/GW170817 with the Giant Metrewave Radio telescope. We began detecting the afterglow at 1390 MHz starting from ~ 65 days since burst and is continuing to follow it up in low radio frequencies. We present 1390 MHz observations up to 152 days since burst. The lightcurve is particularly flat, which may indicate a slow turnover in the flux evolution.

We interpreted the multi-wavelength afterglow in the framework of a structured jet with a Gaussian velocity and energy profile. Bounds on the jet energy, angular structure, observer's viewing angle, and ambient density are obtained through an MCMC parameter estimation. Energy per solid angle at the jet axis is $5.8^{+13.3}_{-3.4} \times 10^{51}$ erg, θ_c is $6.9^{+2.3}_{-1.5}$ degree, θ_v is 27^{+8}_{-5} degree, and ambient density is $0.002^{+0.014}_{-0.002}$ cm^{-3}. The initial bulk Lorentz factor of the jet can not be well constrained, however, a relativistic flow with Γ of a few hundred close to the jet axis is perfectly acceptable. The parameters are consistent with that of typical short-duration GRBs. We find that isotropic energy observed in prompt emission can be reproduced if the total energy budget in prompt emission is an order of magnitude lower than that in the afterglow. Such a difference in energy content between prompt and afterglow is not unusual for GRBs. Our analysis supports the view that GRB 170817A is similar to standard GRBs, with typical energetics and bulk Lorentz factors, except that it is the first clear evidence of a structured outflow.

ACKNOWLEDGMENTS

We thank the staff of the GMRT that made these observations possible. GMRT is run by the National Centre for Radio Astrophysics of the Tata Institute of Fundamental Research.

We thank Avishay Gal-Yam and Doron Kushnir for using the high-performance computing (HPC) facility WEXAC at the Weizmann Institute of Science. The Weizmann HPC facility is partly supported by the Israel Atomic Energy Commission - The Council for Higher Education - Pazi Foundation and partly by a research grant from The Abramson Family Center for Young Scientists.

Development of the BOXFIT code was supported in part by NASA through grant NNX10AF62G issued through the Astrophysics Theory Program and by the NSF through grant AST-1009863. Simulations for BOXFIT version 2 have been carried out in part on the computing facilities of the Computational Center for Particle and Astrophysics (C2PAP) of the research cooperation "Excellence Cluster Universe" in Garching, Germany. This work made use of the IAA-CSIC high performance (HPC) and throughput (HTC) computing infrastructure.

RL acknowledges support from the grant EMR/2016/007127 from Dept. of Science and Technology, India. RL thanks M Govindankutty for generously providing the facilities where part of the computing is done. JB acknowledges support from the CONICYT-Chile grant Basal-CATAPFB-06/2007 and FONDECYT Postdoctorados 3160439. RS-R acknwoledges support from ASI (Italian Space Agency) through the Contract n. 2015-046-R.0 and from European Union Horizon 2020 Programme under the AHEAD project (grant agreement n. 654215). SS acknowledges support from the Feinberg Graduate School.

RS-R thanks for the excellent support and advice from Rafael Parra (Computing Center, IAA-CSIC).

REFERENCES

Abbott, B. P., et al. 2017, Nature, 551, 85

Abbott, B. P., Abbott, R., Abbott, T. D., et al. 2017, Nature, 551, 85

—. 2017a, ApJL, 848, L12

—. 2017b, PhRvL, 119, 161101

Alexander, K., Fong, W., & Berger, E. 2017, GCN Circular, 21589

Arcavi, I., Hosseinzadeh, G., Howell, D. A., et al. 2017, Nature, 551, 64

Blandford, R. D., & McKee, C. F. 1976, Physics of Fluids, 19, 1130

Cenko, S. B., Frail, D. A., Harrison, F. A., et al. 2011, ApJ, 732, 29

Coulter, D. A., Kilpatrick, C. D., Siebert, M. R., et al. 2017a, GCN Circular, 21529

D'Avanzo, P., Campana, S., Ghisellini, G., et al. 2018, A&A, submitted, arXiv:1801.06164

Donaghy, T. Q. 2006, ApJ, 645, 436

Evans, P. A., Cenko, S. B., Kennea, J. A., et al. 2017, Science, 358, 1565

Fong, W., Berger, E., Margutti, R., & Zauderer, B. A. 2015, ApJ, 815, 102

Foreman-Mackey, D., Hogg, D. W., Lang, D., & Goodman, J. 2013, PASP, 125, 306

Frail, D. A., Kulkarni, S. R., Nicastro, S. R., Feroci, M., & Taylor, G. B. 1997, Nature, 389, 261

Goldstein, A., Veres, P., Burns, E., et al. 2017b, ApJL, 848, L14

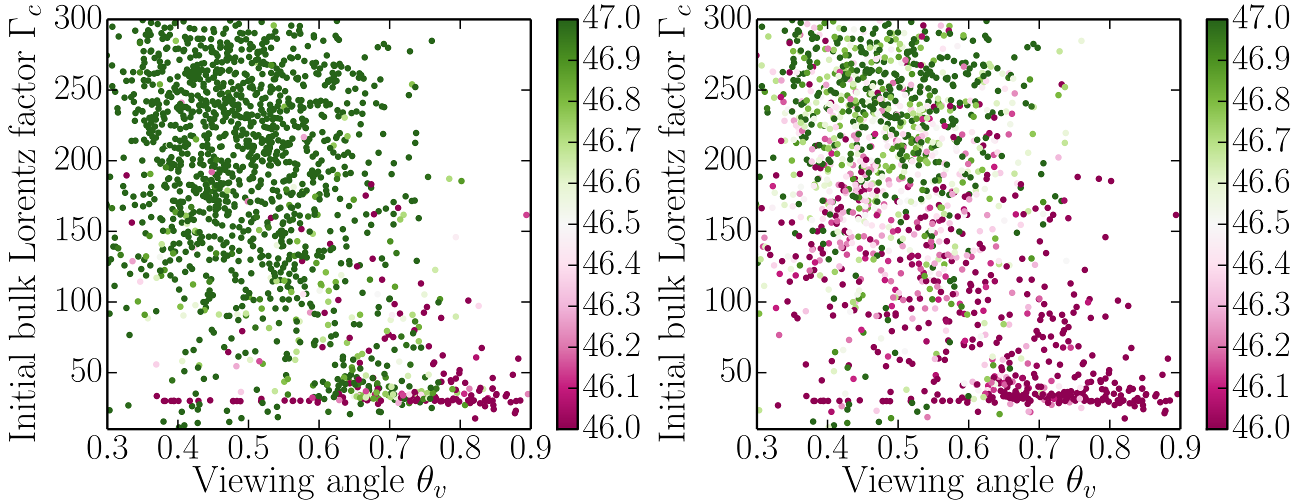

Figure 5. $E^{\gamma}_{\rm iso}$ reproduced by the first 5000 of our high likelihood afterglow solutions. The points are color-coded with the numerically estimated value of $E^{\gamma}_{\rm iso}$. While the afterglow solutions have 4 parameters relevant to the prompt emission ($E_c, \theta_c, \theta_v, \Gamma_c$), we have only shown two dimensions (Γ_c and θ_v) here. The Fermi observed $E^{\gamma}_{\rm iso} = (3.08 \pm 0.72) \times 10^{46}$ erg (Goldstein et al. 2017b) (between 46.4 and 46.6 in log-scale). First panel is for $\zeta = 1$ and the second panel is for $\zeta = 0.1$. A highly relativistic structured outflow can well describe both the prompt and afterglow observations. Nevertheless, the prompt emission seems to have carried relatively less amount of energy than the afterglow.

Granot, J., Gill, R., Guetta, D., & De Colle, F. 2017, MNRAS, submitted, arXiv:1710.06421

Haggard, D., Nynka, M., Ruan, J. J., et al. 2017b, ApJL, 848, L31

Hallinan, G., Corsi, A., Mooley, K. P., et al. 2017, Science, 358, 1579

Hjorth, J., Levan, A. J., Tanvir, N. R., et al. 2017, ApJL, 848, L31

Hotokezaka, K., Kiuchi, K., Shibata, M., Nakar, E., & Piran, T. 2018, ApJ, submitted, arXiv:1803.00599

Kasliwal, M., et al. 2017, GCN Circular, 21552

Kim, S., et al. 2017, Astrophys. J., 850, L21

Lamb, G. P., & Kobayashi, S. 2017, Mon. Not. Roy. Astron. Soc., 472, 4953

Lazzati, D., Perna, R., Morsony, B. J., et al. 2017, Nature, submitted, arXiv:1712.03237

Lipunov, V. M., Gorbovskoy, E., Kornilov, V. G., et al. 2017, ApJL, 850, L1

Lyman, J. D., Lamb, G. P., Levan, A. J., et al. 2018, Nature, submitted, arXiv:1801.02669

Margutti, R., Fong, W., Berger, E., et al. 2017a, GCN Circular, 21648

Margutti, R., Berger, E., Fong, W., et al. 2017b, ApJL, 848, 20

Margutti, R., Alexander, K. D., Xie, X., et al. 2018, ApJ, submitted, arXiv:1801.03531

McMullin, J. P., Waters, B., Schiebel, D., Young, W., & Golap, K. 2007, in Astronomical Society of the Pacific Conference Series, Vol. 376, Astronomical Data Analysis Software and Systems XVI, ed. R. A. Shaw, F. Hill, & D. J. Bell, 127

Mooley, K. P., Hallinan, G., & Corsi, A. 2017a, GCN Circular, 21814

Mooley, K. P., Nakar, E., Hotokezaka, K., et al. 2018, Nature, 554, 207

Nakar, E., & Piran, T. 2018, MNRAS, submitted, arXiv:1801.09712

Pian, E., D'Avanzo, P., Benetti, S., et al. 2017, Nature, 551, 67

Resmi, L., Misra, M., Tanvir, N. R., O'Brian, P., & Schulze, S. 2017a, GCN Circular, 21768

Salafia, O. S., Ghisellini, G., Pescalli, A., Ghirlanda, G., & Nappo, F. 2015, Mon. Not. Roy. Astron. Soc., 450, 3549

Sari, R., Piran, T., & Narayan, R. 1998, ApJL, 497, L17

Soares-Santos, M., Holz, D. E., Annis, J., et al. 2017, ApJL, 848, L16

Swarup, G., Ananthakrishnan, S., Kapahi, V. K., et al. 1991, Current Science, 60, 95

Tanvir, N. R., Levan, A. J., Gonzalez-Fernandez, C., et al. 2017b, ApJL, 848, 27

Taylor, G. 1950, Proceedings of the Royal Society of London Series A, 201, 159

Taylor, G. B., Frail, D. A., Berger, E., & Kulkarni, S. R. 2004, Astrophys. J., 609, L1

Troja, E., & Piro. 2018a, GCN Circular, 22372

Troja, E., & Piro, L. 2018b, The Astronomer's Telegram, 11245

Troja, E., Piro, L., van Eerten, et al. 2017b, Nature, 551, 71

Troja, E., Piro, L., Ryan, G., et al. 2018, MNRAS, submitted, arXiv:1801.06516

van Eerten, H., van der Horst, A., & MacFadyen, A. 2012, ApJ, 749, 44

Waxman, E., Ofek, E., Kushnir, D., & Gal-Yam, A. 2017, ApJ, submitted, arXiv:1711.09638

Wells, D. C. 1985, in Data Analysis in Astronomy, ed. V. di Gesu, L. Scarsi, P. Crane, J. H. Friedman, & S. Levialdi, 195
Yamazaki, R., Yonetoku, D., & Nakamura, T. 2003, ApJ, 594, L79